Protein Density Profile at the Interface of Water with Oligo(ethylene glycol) Self-Assembled Monolayers[†]

M. W. A. Skoda,[‡,§,||] F. Schreiber,[*,§] R. M. J. Jacobs,[⊥] J. R. P. Webster,[||] M. Wolff,[#,▽] R. Dahint,[*,○] D. Schwendel,[○] and M. Grunze[○]

Physical and Theoretical Chemistry Laboratory, South Parks Road, Oxford OX1 3QZ, U.K., Institut für Angewandte Physik, Universität Tübingen, Auf der Morgenstelle 10, D-72076 Tübingen, Germany, Rutherford Appleton Laboratory, Chilton, Didcot OX11 0QX, U.K., Chemistry Research Laboratory, Mansfield Road, Oxford OX1 3TA, U.K., Institut Laue-Langevin, 6, rue Jules Horowitz, BP 156-38042 Grenoble Cedex 9, France, Institute for Experimental Physics/Solid-State Physics, Ruhr-University Bochum, D-44780 Bochum, Germany, and Lehrstuhl für Angewandte Physikalische Chemie, Ruprecht-Karls-Universität Heidelberg, Im Neuenheimer Feld 253, D-69120 Heidelberg, Germany

Received August 31, 2008. Revised Manuscript Received November 25, 2008

We determined the density profile of a high-molecular-weight globular protein (bovine serum albumin, BSA) solution at the methoxy tri(ethylene glycol)-terminated undecanethiol SAM/protein solution interface by neutron reflectivity measurements. Information about the interactions between oligo(ethylene glycol) (OEG)-terminated self-assembled monolayers (SAMs) and proteins is derived from the analysis of the structure of the solid−liquid interface. The fitting results reveal oscillations of the protein density around the bulk value with decaying amplitude on a length scale of 4 to 5 nm. The amplitude, phase, period, and decay length are found to vary only slightly with temperature and the ionic strength of the protein solution. Adsorption is reversible within the limits of detection, which suggests that the hydrated ethylene glycol surface inhibits the protein from unfolding and irreversible bonding. The insensitivity of BSA adsorption toward the ionic strength of the solution contrasts with observations in surface force experiments with a fibrinogen-coated AFM tip, where electrostatic repulsion dominates the protein/OEG SAM interaction. As reported previously, irreversible BSA adsorption takes place below 283 K, which we interpret as indicative of the presence of dynamic effects in the protein resistance of short-chain OEG-terminated surfaces.

Introduction

The study of interfaces and interfacial phenomena in the fields of bioscience and nanoscience, especially of interfaces between artificial and biological media, is of tremendous importance.[1−5] Specifically, oligo(ethylene glycol) (OEG) and poly(ethylene glycol) (PEG) are materials relevant in biotechnological applications, such as biosensing,[6,7] and in supporting model membranes.[8,9] In particular, it has been found that OEG- and PEG-coated surfaces are resistant to irreversible protein adsorption,[10] although the underlying physicochemical mechanisms of this resistance are still under discussion. Whereas resistance to protein adsorption by end-grafted high-molecular-weight PEG can be theoretically explained by the unfavorable free-energy change caused by dehydration and steric confinement of the swollen polymer,[11,12] the same arguments appear not to be valid for the densely packed and conformationally restricted OEG-terminated undecane thiolate SAMs.

The protein resistance of OEG-terminated SAMs, that is, complete reversibility of adsorption, was first reported in the seminal paper by Prime and Whitesides,[10] and it was suggested that protein resistance is of entropic origin. Extensive and detailed analysis of the packing density and molecular conformation in OEG-terminated SAMs, measured on dry films, led to the conclusion that because of the conformational constraints imposed by dense packing, an entropic mechanism of protein resistance is unlikely.[13] The importance of water penetration into the OEG terminus of the films to render them protein-resistant was established only later.[14,15] The penetration of water into OEG-terminated SAMs was recently demonstrated independently by PM-IRRAS.[16] It was suggested that the unfavorable change in free energy when removing the strongly bound water in the interface[17,18] could prevent the proteins from adsorbing as a result of attractive van der Waals interactions.

[†] Part of the Neutron Reflectivity special issue.
* To whom correspondence should be addressed.
[‡] Physical and Theoretical Chemistry Laboratory.
[§] Universität Tübingen.
[||] Rutherford Appleton Laboratory.
[⊥] Chemistry Research Laboratory.
[#] Institut Laue-Langevin.
[▽] Ruhr-University Bochum.
[○] Ruprecht-Karls-Universität Heidelberg.

(1) Schreiber, F. *Prog. Surf. Sci.* **2000**, *65*, 151–257.
(2) Schreiber, F. *J. Phys.: Condens. Matter* **2004**, *16*, R881−R900.
(3) Vogler, E. A. *J. Biomater. Sci. Polym. Ed.* **1999**, *10*, 1015–1045.
(4) Ball, P. *Nature* **2003**, *423*, 25–26.
(5) Chandler, D. *Nature* **2005**, *437*, 640–647.
(6) Riepl, M.; Enander, K.; Liedberg, B.; Schäferling, M.; Kruschina, M.; Ortigao, F. *Langmuir* **2002**, *18*, 7016–7023.
(7) Svedhem, S.; Ohberg, L.; Borrelli, S.; Valiokas, R.; Andersson, M.; Oscarson, S.; Svensson, S.; Liedberg, B.; Konradsson, P. *Langmuir* **2002**, *18*, 2848–2858.
(8) Lahiri, J.; Kalal, P.; Frutos, A.; Jonas, S.; Schaeffler, R. *Langmuir* **2000**, *16*, 7805–7810.
(9) Jenkins, A.; Bushby, R.; Evans, S.; Knoll, W.; Offenhäusser, A.; Ogier, S. *Langmuir* **2002**, *18*, 3176–3180.
(10) Prime, K. L.; Whitesides, G. M. *J. Am. Chem. Soc.* **1993**, *115*, 10714–10721.
(11) Jeon, S. I.; Lee, J. H.; Andrade, J. D.; de Gennes, P. G. *J. Colloid Interface Sci.* **1990**, *142*, 149–157.
(12) de Gennes, P. *Macromolecules* **1981**, *14*, 1637–1644.
(13) Harder, P.; Grunze, M.; Dahint, R.; Whitesides, G. M.; Laibinis, P. E. *J. Phys. Chem. B* **1998**, *102*, 426–436.
(14) Zolk, M.; Eisert, F.; Pipper, J.; Herrwerth, S.; Eck, W.; Buck, M.; Grunze, M. *Langmuir* **2000**, *16*, 5849–5852.
(15) Pertsin, A.; Hayashi, T.; Grunze, M. *J. Phys. Chem. B* **2002**, *106*, 12274–12281.
(16) Skoda, M.; Jacobs, R.; Willis, J.; Schreiber, F. *Langmuir* **2007**, *23*, 970–974.
(17) Wang, R.; Kreuzer, H.; Grunze, M. *J. Phys. Chem. B* **1997**, *101*, 9767–9773.
(18) Wang, R. L. C.; Kreuzer, H.; Grunze, M. *Phys. Chem. Chem. Phys.* **2000**, *2*, 3613–3622.

10.1021/la8028534 CCC: $40.75
Published on Web 02/05/2009

A different mechanism to explain protein repulsion was suggested from the observation of long-range repulsive electrostatic forces between fibrinogen-coated AFM tips and protein-resistant methoxy-tri(ethylene glycol)-terminated undecanethiolate SAMs on Au (Au/S-$(CH_2)_{11}(OCH_2CH_2)_3$-OCH_3), abbreviated EG3OMe.[19] The measured repulsive potential scaled with the Debye length of the solution. In addition, a negative surface potential on these SAMs was measured in streaming potential experiments.[20] It was suggested that the negative surface potential arises from a tightly bound layer of hydroxide ions that are immobilized by stabilizing their hydration shell via inclusion of water molecules strongly hydrogen bonded to the OEG moieties of the film.[21,22]

The repulsive forces observed in AFM measurements can rationalize the protein-resistant character of the SAMs, but the principal drawback of this experimental technique is that it does not mimic the situation for a native protein rotating and moving freely in solution. The AFM experiment rather probes the interaction of a irreversible bound protein, that is, with a spatially fixed and non-native secondary structure, with the substrate. In particular, the absence of free rotation and thus the ability to assume a low-energy orientation with respect to the surface force fields will alter the force balance and their magnitude between the solute and the surface. It may therefore be that the electrostatic mechanism inferred from the AFM force measurements is not really relevant to the interaction of a free protein molecule with the OEG surfaces. Thus, because numerous factors obviously contribute to protein resistance, the issue of the provenience of protein resistance in OEG SAMs remains a subject of controversy.[21,23]

This article elaborates on the interactions that are present between OEG SAMs and high-molecular-weight globular protein bovine serum albumin (BSA) in solution by experiments that are able to distinguish between repulsive forces leading to an effective depletion of protein concentration on the surface and completely reversible adsorption.

In general, there are three possible scenarios for protein interaction with a surface:

(i) The protein adsorbs onto the surface and becomes irreversibly bound by either strong hydrophobic or electrostatic interactions or by chemical bond formation between the denatured protein and the substrate.

(ii) The proteins adsorb reversibly on the surface and can be removed, for instance, by applying a shear force parallel to the surface, such as in rinsing processes. Reversible (weak) adsorption implies either a balance of prevailing attractive and repulsive physical forces or the inability of the protein to form irreversible bonds to the hydrated OEG surface. Note that the energy necessary to remove an adsorbed protein is usually on the order of k_BT,[24] and hence an equilibrium state will be established between adsorption and desorption. In this context, we recall that in situ SPR experiments showing reversible adsorption, that is, the protein can be completely rinsed off the surface by replacing protein solution with buffer, do not allow one to distinguish between the protein being repelled from the surface or being reversibly adsorbed.

(iii) There is no adsorption at all, and the proteins remain in solution.

It is improtant to note that most state-of-the-art experiments showing protein resistance are based on the observation that no protein is detected on the surface after replacing protein solution with buffer and rinsing. Thus, ex situ experiments do not allow one to distinguish between the protein being repelled from the surface (case (iii)) or being reversibly adsorbed (case (ii)).

The mechanisms leading to adsorption of type (i) are mostly due to van der Waals, electrostatic, and hydrophobic interactions and have been documented in the literature.[11,24] As already mentioned, the second case of reversible adsorption is very difficult to quantify and to distinguish from case (iii). For the case where no adsorption occurs, some repulsive interaction has to be assumed because it is competing against the omnipresent attractive (van der Waals and hydrophobic) interactions between protein and substrate. This repulsive interaction can be electrostatic, entropic, or enthalpic in nature or a mixture of these. Electrostatic and entropic interactions are fundamentally different, with the former being of long-range and the latter being roughly on the order of the diameters of the objects involved. Energy contributions could arise from the change in free energy due to the dislocation of tightly bound water molecules during the adsorption process. Furthermore, the effective range of the electrostatic interaction depends on other charges that are present, which have a screening effect. Thus, the strongest interaction is expected when there are no charges in the solution. Entropic forces are more complex and depend strongly on the specific details of the system, such as geometry and chemical potentials, and it is difficult to formulate a generic description.

The assumption of electrostatic repulsive forces between proteins and OEG-terminated surfaces (case (iii)) has two major consequences: the electrostatic potential will establish a characteristic density distribution function of the proteins in solution, and this function will strongly depend on the ionic strength of the solution. The density function and its range have been calculated from the results obtained by Feldmann et al.[19] in their AFM experiments, and the repulsive force can be fitted by an exponential function

$$F(z) = A \exp(-z/z_0) \tag{1}$$

where $A = 0.8$ nN is the force experienced right at the surface and $z_0 = 18.67$ nm is its decay length. The repulsive force creates a protein flow away from the surface, which is balanced by diffusion toward the surface along the concentration gradient. Considering also frictional forces experienced by the moving proteins, the following differential equation has to be solved for the equilibrium case:

$$\frac{dn(z)}{dz} = \frac{A}{6\pi\eta r D} n(z) \exp(-z/z_0) \tag{2}$$

Here, $n(z)$ denotes the protein number density at distance z from the surface, r is the protein radius, D is its diffusion coefficient, and η is the viscosity of the solvent. This yields

$$n(z) = n_\infty \exp(-Bz_0 \exp(-z/z_0)) \tag{3}$$

for the protein concentration as a function of distance from the interface. n_∞ is the bulk concentration in the solution and $B = A/6\pi\eta r D$. The calculated value for B for a 15 wt % concentrated BSA solution, as used in the present reflectivity experiments, is 16.17 Å^{-1}. The concentration profile of the protein solution can now be easily calculated (Figure 1). The calculated profiles show that, depending on the decay length that is assumed, there is a

(19) Feldman, K.; Hähner, G.; Spencer, N. D. M.; Harder, P.; Grunze, M *J. Am. Chem. Soc.* **1999**, *121*, 10134–10141.
(20) Chan, Y.-H.; Schweiss, R.; Werner, C.; Grunze, M. *Langmuir* **2003**, *19*, 7380–7385.
(21) Herrwerth, S.; Eck, W.; Reinhardt, S.; Grunze, M. *J. Am. Chem. Soc.* **2003**, *125*, 9359–9366.
(22) Kreuzer, H.; Wang, R.; Grunze, M. *J. Am. Chem. Soc.* **2003**, *125*, 8384–8389.
(23) Kane, R.; Deschatelets, P.; Whitesides, G. *Langmuir* **2003**, *19*, 2388–2391.
(24) Roth, C. M.; Lenhoff, A. M. *Langmuir* **1993**, *9*, 962–972.

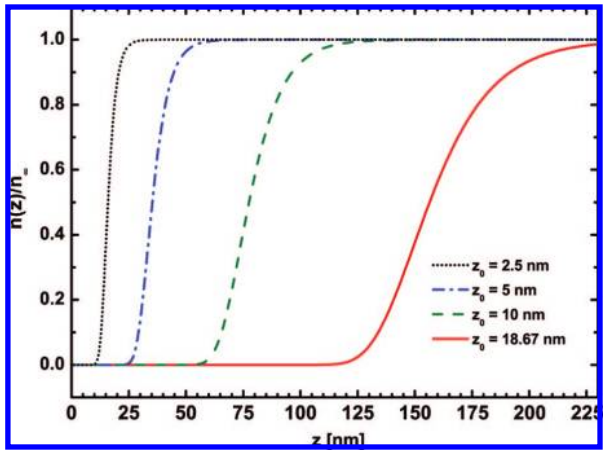

Figure 1. Calculated protein density profiles (normalized to bulk density) for an EG3OMe-terminated surface in contact with a 15 wt % BSA solution based on the force−distance measurements of Feldman et al.[19] The value of $z_0 = 18.67$ nm is directly extracted from the AFM measurements. Three other decay constants are shown for comparison.

region of approximately 10−100 nm with almost vanishing protein concentration, followed by a steep rise to the bulk value of the concentration. Assuming electrostatic interactions, the decay length will scale with the Debye length of the solution, and the extent of the protein-depleted region should vary as a function of the ionic strength. The neutron reflectivity experiments presented in this article aim to measure the density profile close to the interface of protein solutions in contact with protein-resistant OEG-terminated monolayers in order to elucidate the mechanisms of interaction.

Experimental Section

Chemicals. The following thiols have been obtained from the sources given and were used as received: HS-$(CD_2)_{17}$-CD_3 and HS-$(CD_2)_{12}$-$(O\text{-}CD_2\text{-}CD_2)_3$-$OCD_3$ was obtained from ProChimia, Poland, and HS-$(CH_2)_{11}$-$(O\text{-}CH_2\text{-}CH_2)_3$-$OCH_3$ (EG3OMe) was synthesized following procedures described in refs 10 and 25. HS-$(CH_2)_{13}$-CH_3 (C14) (product no. 87193) was purchased from Sigma-Aldrich and used as received. Absolute ethanol purissimum pro analysi was purchased from Riedel-de-Haën and used as received. Bovine serum albumin (BSA) (product no. A7638) was purchased from Sigma-Aldrich. This lyophilized powder with a molecular weight of ∼66 kDa was used as received. Lysozyme (LYS) from chicken egg white (product no. L6876) was purchased from Sigma-Aldrich and used as received.

Substrates. Polished, large-area (100 × 80 mm^2), single-crystal (001) SiO_2 (quartz) blocks with a thickness of 12.7 mm were purchased from CrysTec, Berlin, Germany. The root-mean-square (rms) roughness was about 0.1−0.2 nm (sometimes less) as determined by AFM over an area of 1 μm^2. The quartz blocks were first thermally evaporated with a layer of either 1−2 nm of Ti or 5−10 nm of Cr in order to promote the adhesion of the subsequently deposited Au layer. Au layer thicknesses ranged from 35 to 70 nm and were controlled by a quartz crystal microbalance (XTC Inficon, Leybold, Germany). Prior to evaporation, the blocks were oxygen plasma cleaned to remove any organic impurities from the surface. The Au-coated samples were stored under argon until further use.

SAM Formation and Characterization. All glassware used to prepare the samples were left overnight in hydrogen peroxide and rinsed with ethanol p.a. The Au-coated quartz blocks were cleaned in a home-built ozone producing reactor (using a Heraeus Noblelight UV lamp) for 1 h. After the samples had cooled, they were thoroughly rinsed with ethanol and immediately submerged in a 500 μM ethanolic solution of the respective thiol. The solution containing the sample was stored at room temperature with typical incubation times in excess of 20 h. Afterward, the sample was carefully removed from the thiol solution and immediately copiously rinsed with absolute ethanol in order to remove physisorbed molecules. The sample was then blow dried in a gentle argon stream and stored under argon until use. Successful SAM formation was verified by grazing-angle polarization-modulation infrared spectroscopy with a BioRad FTS 6000 spectrometer.

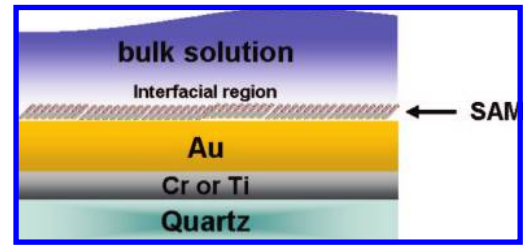

Figure 2. Generic arrangement of layers on which the fitting model was based (not to scale).

Neutron Reflectivity. Neutron reflectivity measurements were performed on the ADAM reflectometer[26,27] at the Institut Laue-Langevin in Grenoble, France. The sample geometry was vertical, a fact that minimized the influence of potential air bubble formation on the sample. The neutron wavelength was $\lambda = 4.41$ Å with a resolution of $\Delta\lambda/\lambda = 0.006$. The collected reflectivity data were footprint corrected, and true specular information was obtained by measuring the reflectivity on the specular path and then subtracting the off-specular reflectivity measured with the sample angle offset by $\Delta\theta$ from the specular condition. $\Delta\theta$ for each sample was determined by rocking scans at several different Q_z values. (Q_z is the out-of-plane momentum transfer.) The width Δw of the rocking (specular) peak was determined, and the offset was set to $\Delta\theta = 2\Delta w$. Additional experiments were performed at the ISIS pulsed neutron source on the SURF reflectometer[28] and on the SPEAR reflectometer at LANSCE.

Data Fitting and Interpretation

The resulting curves were fitted using the Parratt32 software,[29] which calculates the reflectivity profile using Parratt's recursive method based on a multiple-box model. The box model includes three parameters for each layer: thickness, scattering length density, and roughness. The starting values for the thickness of the metal layers in the model were taken from the quartz crystal microbalance readings during the evaporation process and were confirmed by measuring the X-ray reflectivity using a Bruker D8 Advance diffractometer. The base model consisted of the following layers (Figure 2): a quartz substrate, an adhesion promoter (either Cr or Ti), Au, SAM, and the bulk protein solution. One or more additional layers were introduced between the SAM and the bulk to account for interfacial density fluctuations in the protein solution. However, it was found that the protein density profile could be described most satifactorily and with the least number of parameters by a decaying, oscillating analytical profile function (see below). During the fitting procedure, the scattering length density, thickness, and roughness parameters of each

(25) Pale-Grosdemange, C.; Simon, E. S.; Prime, K. L.; Whitesides, G. M. *J. Am. Chem. Soc.* **1991**, *113*, 12–20.

(26) Schreyer, A.; Siebrecht, R.; Englisch, U.; Pietsch, U.; H., Z. *Physica B* **1998**, *248*, 349–354.

(27) Wolff, M.; Zhernenkov, K.; Zabel, H. *Thin Solid Films* **2007**, *515*, 5712–5715.

(28) Bucknall, D. G.; Penfold, J.; Webster, J. R. P.; Zarbakhsh, A.; Richardson, R. M.; Rennie, A.; Higgins, J. S.; Jones, R. A. L.; Fletcher, P.; Thomas, R.; Roser, S.; Dickinson, E. *ICANS-XIII* **1995**, 123–129.

(29) Braun, C. *Parratt32*, version 1.6; www.hmi.de/grossgeraete/bensc.

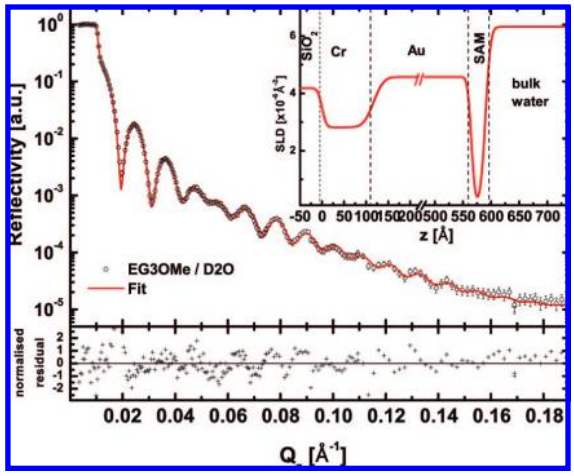

Figure 3. Typical neutron reflectivity measurement. An EG3OMe-terminated monolayer is measured in contact with D_2O. The fit (red solid line), real space profile (inset), and normalized residual ($[R_{exp}(Q_i) - R_{calc}(Q_i)]/\delta_{exp}(Q_i)$) are also shown.

individual layer were allowed to vary. After the fit had converged, the χ^2 value

$$\chi^2 = \sum_i \frac{(R_{exp}(Q_{z,i}) - R_{calc}(Q_{z,i}))^2}{\delta_{exp}{}^2(Q_{z,i})} \quad (4)$$

was noted and used to find the best model as described in the following text. In eq 4, $R_{exp}(Q_{z,i})$ is the reflectivity value measured at $Q_{z,i}$, $R_{calc}(Q_{z,i})$ is the calculated value according to the respective model, and $\delta_{exp}{}^2(Q_{z,i})$ represents the statistical error, taken to be the square root of the count rate. To determine the quality of the model, fits with an increasing number of parameters (e.g., an oscillating, decaying function) were carefully analyzed using the N_σ qualifier[30]

$$N_\sigma = \frac{\chi^2 - \nu}{\sqrt{2\nu}} \quad (5)$$

where X^2 is the error-weighted least-squares sum and $\nu = n - p$ is the effective number of degrees of freedom, with n being the number of data points used for the fit and p being the number of fitting parameters. (This procedure is illustrated in Figure 3.) Small values of N_σ indicate a high probability for the assumed model. This quantity is derived from the properties of the χ^2 distribution and can be calculated easily. A comparison of N_σ for two models with different numbers of parameters is comparable with the so-called Hamilton test,[31] in which the ratio

$$\mathcal{R} = \sqrt{\frac{\chi_0^2}{\chi_{n/\text{oscill}}^2}} \quad (6)$$

Is computed and the result is compared with tabulated values of confidence intervals. Here, $\chi_0{}^2$, $\chi_n{}^2$ and $\chi_{oscill}{}^2$ are the least-squares sums for the models without and with n additional layers (n-box model) or an oscillating profile function, respectively. The tabulated $\mathcal{R}$ values were interpolated for the appropriate degrees of freedom of each individual fit using the interpolation formula (Ib) from ref 31

$$\mathcal{R}_{b,\nu,\alpha} \simeq 1 + \frac{120}{\nu}(\mathcal{R}_{b,120,\alpha} - 1) \quad (7)$$

where ν is, as before, the actual effective number of degrees of freedom, b is the difference in the number of parameters between the two compared models, and α is the confidence band, which was in all cases $\alpha = 0.005$, meaning that the model without the additional layer could be rejected with a probability of 99.5% if $\mathcal{R} > \mathcal{R}_{b,\nu,\alpha}$. Both N_σ and the Hamilton test were used to compare models with differing numbers of parameters and to reject the more improbable model with high confidence. By carefully checking these criteria, we have made sure that the essence of the physics is captured while keeping the model as simple as possible.

Results and Discussion

Calibration of Sensitivity. The system that we study in this work is composed of the quartz substrate, Cr (or Ti) and Au layers, the SAM, and the liquid phase. Its complexity is further increased when studied in contact with proteins in solution. The phase behavior and interaction potentials of the free proteins in solution as a function of protein and salt concentration are known from our previous studies.[32] The experimental sensitivity was increased by contrast matching of SAM and solutions, and complementary adsorption studies served to calibrate the achievable resolution for the studied system. (See the following paragraph.) With these prerequisites, it is possible to study the structure of the solid/liquid interface between OEG SAMs and protein solutions with high accuracy.

Proteins such as BSA or lysozyme will adsorb on noninert surfaces as discussed in the introduction. To calibrate the sensitivity limits of the system, an identical system was used where the protein-resistant OEG-terminated SAM was replaced by a nonresistant alkanethiol ($HS\text{-}(CD_2)_{17}\text{-}CD_3$) SAM of similar thickness. The amount of adsorbed protein is known from other studies, such as Silin et al.,[33] where the fractional coverage of adsorbed BSA on a CH_3-terminated alkanethiol SAM is about 0.23 of a monolayer (~80 ng/cm^2) and for lysozyme approximately 0.26 of a monolayer (~100 ng/cm^2),[34] depending on pH. Therefore, measurements on this known system are used to determine to what extent an additional layer affects the reflectivity profile and how sensitive the subsequent fitting routines are to these subtle changes. Prior to the adsorption experiment with a 2 mg/mL lysozyme solution in D_2O, reflectivity data of the same sample were taken in contact with an H_2O/D_2O mixture, adjusted to match the scattering length density of the protein solution. Thus, the two data sets can be compared immediately: in the case of no changes at the solid−liquid interface, H_2O/D_2O and the protein data set should be identical. However, any changes in the density profile at the interface should cause changes in the measured reflectivity profile. An example of such a measurement is shown in Figure 4. The real-space profile of the measurement against H_2O/D_2O shows a sharp dip next to the SAM, which can be interpreted as a reduced density water layer caused by the hydrophobic SAM, although the extent of such a layer is still very controversial. The fit for the measurement with the lysozyme solution reveals an additional layer: an adsorption layer (dip in the scattering length density (SLD) profile) of about 2.6 nm thickness and a scattering length density of 5.0×10^{-6} Å^{-2}, corresponding to a surface coverage of adsorbed lysozyme of

(30) Ihringer, J. *J. Appl. Crystallogr.* **1995**, *28*, 618–619.
(31) Hamilton, W. C. *Acta Crystallogr.* **1965**, *18*, 502–510.
(32) Zhang, F.; Skoda, M.; Jacobs, R.; Martin, R.; Martin, C.; Schreiber, F. *J. Phys. Chem. B* **2007**, *111*, 251–259.
(33) Silin, V.; Weetall, H.; Vanderah, D. *J. Colloid Interface Sci.* **1997**, *185*, 94–103.
(34) Luk, Y.-Y.; Kato, M.; Mrksich, M. *Langmuir* **2000**, *16*, 9604–9608.

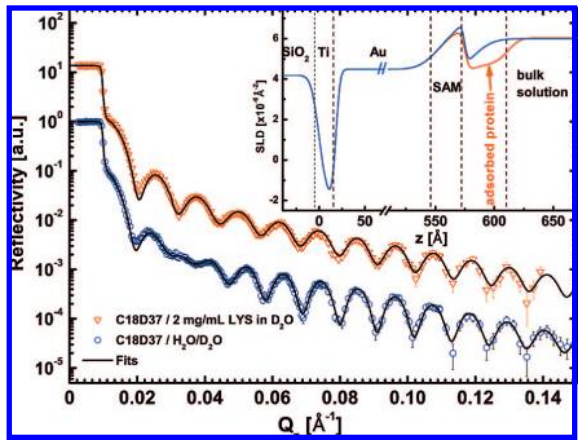

Figure 4. Measured reflectivity curves and fitted real-space profiles (inset) for a deuterated octadecyl thiolate SAM in contact with an H_2O/D_2O mixture (blue circles) and in contact with a 2 mg/mL lysozyme (LYS) solution with an identical scattering length density (orange triangles). The fit for the lysozyme measurement shows an adsorbed layer of about 2.6 nm thickness and a coverage of about 0.3 of a monolayer. The curves are offset vertically by a factor of 10.

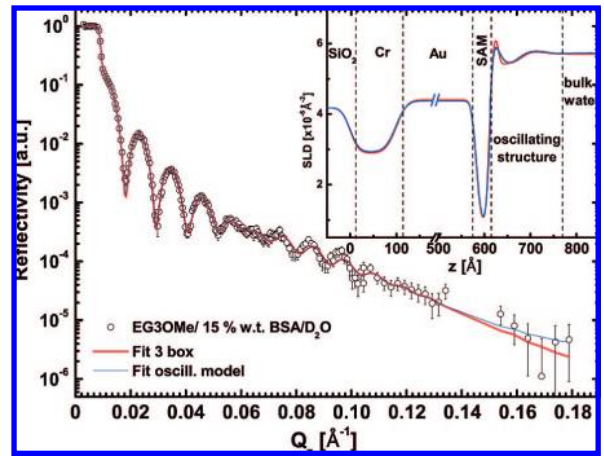

Figure 5. Reflectivity data with the best fit and corresponding scattering length density profiles for a sample of an EG3OMe SAM in contact with a 15 wt % BSA/D_2O solution at room temperature. The real-space profile shows an oscillatory structure of the protein density profile adjacent to the SAM, both when fitted with a 3-box model or with an oscillating analytical profile function. For exact fitting results, see Table 1.

Table 1. Fit Parameters for the Fits in Figure 5 Using 2- and 3-Box Models as Well as an Analytical Oscillating Function[a]

layer	d (nm)	SLD ($\times 10^{-6}$Å^{-2})	σ (nm)
quartz	n/a	4.18	n/a
Cr	9.90	2.93	1.47
Au	48.26	4.41	1.86
SAM	2.90	0.96	0.13
layer 0	1.87	6.18	0.83
layer	5.36	5.47	1.20
depletion layer	3.31	5.90	1.98
oscillating decay: $A = 0.92 \times 10^{-6}$ Å^{-2}, $\lambda_p = 11.68$ nm, $\phi = 1.95$, $\xi = 3.78$ nm			
bulk	n/a	5.71	3.29
Hamilton 2 box: $b = 3$, $\nu = 199$; $\mathcal{R}_{3,\,199,\,0.005} = 1.036$, $\mathcal{R} = (\chi_1^2/\chi_2^2)^{1/2} = 1.189$			
Hamilton 3 box: $b = 3$, $\nu = 197$; $\mathcal{R}_{3,\,197,\,0.005} = 1.036$, $\mathcal{R} = (\chi_2^2/\chi_3^2)^{1/2} = 1.037$			
Hamilton oscill.: $b = 3$, $\nu = 199$; $\mathcal{R}_{3,\,199,\,0.005} = 1.036$, $\mathcal{R} = (\chi_1^2/\chi_{oscill}^2)^{1/2} = 1.382$			
N_σ test: $N_\sigma^3 = 12.61$, $N_\sigma^2 = 12.66$, $N_\sigma^1 = 21.53$, $N_\sigma^{oscill} = 6.91$			

[a] Confidence tests strongly reject 1- and 2-box models with a probability of 99.5%. The N_σ qualifier strongly favors the model with the analytical oscillating function.

approximately 0.3 of a monolayer. The integrated area of this layer is $A = 25 \times 10^{-6}$ Å^{-1}. (The real-space profile resulting from the best fit was integrated numerically as the area below the bulk water value of the scattering length density profile between the end of the SAM and the beginning of the bulk.) These values serve as a benchmark for the sensitivity of the measurement: a change of this magnitude in the density profile produces very easily discernible changes in the reflectivity curve (at low Q_z), and it can be extrapolated that even smaller effects, on the order of $A = 10 \times 10^{-6}$ Å^{-1} for the integrated area, are easily detected.

Density Profiles. To avoid ambiguity for the fitted neutron reflectivity profiles, prior to each measurement with protein solutions, a measurement of the same system was performed with pure D_2O. This reference profile was fitted, and subsequent data were fitted using the parameters for the Cr (Ti) and Au layers as obtained from the reference measurement as fixed values. As a check, after the fit had converged, the parameters for the metal layers were also included in the fit. These refined values for Cr (Ti) and Au did not differ by more than ±0.2 nm.

The subsequent measurement was performed using a 15 wt % concentrated BSA/D_2O solution (Figure 5). The relatively high protein concentration was necessary to achieve a sufficiently high contrast in the case of a protein-depleted layer.

In the fitting model, one and two additional layers were introduced to account for changes at the solid/liquid interface. The goodness of fit and likelihood of the 1-, 2-, and 3-box models were compared using Hamilton and N_σ tests.

All data sets involving protein solutions could be fitted most satisfactorily by using a three-layer model with an oscillatory structure: adjacent to the SAM, a layer with increased scattering length density is observed, followed by a region where the scattering length density is lower than that of the bulk phase. Then a layer with increased density compared to the bulk value follows (indicating a more or less pronounced reduction in protein density), which extends up to about 4−6 nm into the bulk solution. This characteristic behavior is illustrated in Figure 5. Note that the generic behavior is similar for both the 3-box model and the oscillating decay model (see below): starting from the SAM, the regions with increased and reduced scattering length density are of the same order. The advantage of the oscillating analytical profile function is the smaller number of parameters and the fact that it is physically more meaningful.

Oscillating Decay Model. It is important to note that for a concentrated (15 wt %) aqueous protein solution a reduced scattering length density compared to the bulk value represents a locally higher protein concentration whereas a value above the bulk scattering length density is equivalent to a lower protein density. Because the obtained real-space profiles suggest an oscillating behavior of the protein density at the SAM/solution interface, a model with an analytical profile function was employed. In particular, an oscillating sinusoidal function with damped amplitude was used to describe the scattering length density profile of the solution close to the SAM

$$SLD(z) = A \sin\left(\frac{2\pi}{\lambda_p} z + \phi\right) e^{-z/\xi} \qquad (8)$$

where A is the amplitude of the oscillation, λ_p is its wavelength, ϕ is the phase, and ξ is the decay constant for the damping. The analytical function was split into 0.2-nm-wide boxes with zero roughness within the Parratt32 fitting software. The roughness

of the bulk layer was kept at zero such that the resulting model has a total of 18 parameters (including substrate, solution, and metal-layer parameters), which is the same number of parameters as for a 2-box model. The new model with the analytical function was found to converge more reliably, and the parameters (A, λ_p, ϕ, and ξ) are better suited to the comparison of fits from different data sets. An oscillating decay model is more appropriate for describing the layering of hard spheres in the vicinity of a hard wall.[35−38] The oscillation period in hard sphere liquids with high packing fractions is on the order of the hard sphere diameter, hence it is to be expected that for a more dilute solution the period will tend toward a value similar to the average interparticle spacing. The period observed in the neutron reflectivity measurements lies in the range of 10.3−10.8 nm for a 15 wt % BSA solution. This value is in excellent agreement with the average interparticle spacing obtained from the SAXS measurements of BSA in solution:[32] the maximum of the scattering intensity at 200 mg/mL (which is close to a concentration of 15 wt %) is at approximately $Q_z = 0.06$ Å^{-1}, which corresponds to an average interparticle distance of $2\pi/Q_z \approx 10.5$ nm. The protein-depleted region extends only 3 to 4 nm from the SAM and is followed by a maximum in protein concentration. The radius of BSA, having a similar value, may indicate that the proteins reach the proximity of the SAM but are prevented from adsorbing irreversibly, for instance, by a strongly bound hydration layer. This observation is in agreement with SAXS studies of mixtures of BSA and OEG-functionalized Au nanoparticles.[39] Protein resistance of the OEG-decorated nanoparticles was observed, and the protein-resistant nanoparticles showed a high colloidal stability up to high salt concentrations (2.0 M). Furthermore, our reflectivity study shows that the overall period of oscillation of the protein density is similar to the protein diameter. However, further studies are necessary to reveal a quantitative relationship between oscillation parameters and solution characteristics, such as protein size, concentration, protein charge, and so forth.

A comparison of the oscillating decay model with a 3-box model is presented in Figure 6. The parameters of the SAM, in particular, the roughness, that were also allowed to vary during the fitting process are more realistic in the oscillating model fit (Table 1).

The fit parameters of the analytical function were determined to be $A = 0.92 \times 10^{-6}$ Å^{-2}, $\lambda_p = 11.68$ nm, $\phi = 1.95$, and $\xi = 3.78$ nm. The oscillating protein density distribution function at the SAM/solution interface is characteristic of the behavior of a (charged) hard sphere mixture at a hard wall. It should be noted that BSA has a maximum dimension of 8 to 9 nm[40,41] and the interparticle spacing at this concentration (15 wt %) is about 11 to 12 nm.[32] The region closest to the SAM has a scattering length density of around 6×10^{-6} Å^{-2} and a width of approximately 3 nm, which is consistent with a protein-depleted region with reduced water density (SLD $= 6.18 \times 10^{-6}$ Å^{-2}, which is about 97% of the bulk density) as also observed in ref 42. The following dip in the density profile down to $\sim 5.5 \times 10^{-6}$ Å^{-2} with an extent of about 3 to 4 nm indicates a slightly higher protein concentration compared to that of the bulk: a volume fraction of ~0.2 can be calculated from the scattering length densities of BSA and D_2O whereas the bulk volume fraction is about 0.13. The next protein-depletion region is less pronounced than the first one, and the oscillations are damped out quickly after approximately 15−18 nm.

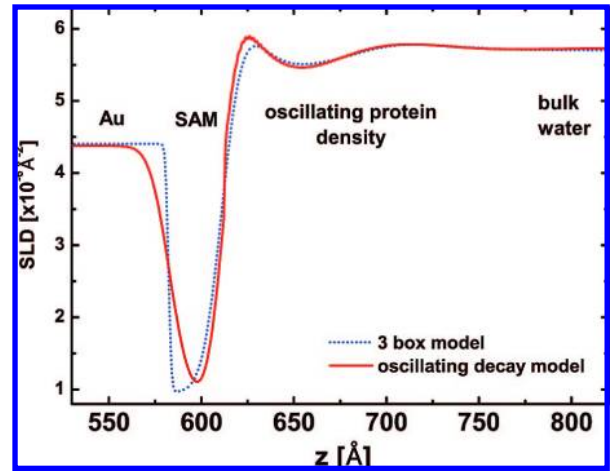

Figure 6. Comparison of a 3-box fitting model with an oscillating decay model ($SLD(z) = A \sin((2\pi)/(\lambda_p)z + \phi)e^{-z/\xi}$) for the data set shown in Figure 5. In the fitting process, the SAM parameters were also allowed to vary. Both models are very similar and show the oscillating structure of the protein density close to the SAM. The parameters of the analytical function are listed in Table 1.

Sensitivity of Models. The most suitable model for describing the protein density at the solid/liquid interface is a damped oscillating function with the following four parameters: amplitude A, period and phase of the oscillation λ_p and ϕ, respectively, and decay length ξ. This model was chosen because it described the profile with fewer parameters than did a 3-box model and yielded the best goodness of fit. However, it is a rather complex model; therefore, a brief discussion of the sensitivity of the parameters is given in this section. For this purpose, by taking a typical measurement (from Figure 5), each parameter is varied stepwise while keeping all other parameters fixed, and the resulting χ^2 values are plotted against the parameter value (Figure 7). From the plots, it can be deduced that the period and phase are found in a well-defined minimum whereas the amplitude and the decay length of the density oscillation have somewhat broader minima. Following these considerations, the errors in the fitted values can be calculated from the plots in Figure 7 on the basis of the parameter value obtained when the normalized χ^2 increased by 10%. The fitted values for the oscillating decay parameters have the following errors: period $\lambda_p = (10.88 \pm 0.80)$ nm, decay length $\xi = (5.83 \pm 1.30)$ nm, amplitude $A = (6.519 \pm 1.250) \times 10^{-7}$ Å^{-2}, and phase $\phi = (1.281 \pm 0.175)$. These values for the fitting errors are representative of all presented measurements. The phase is the most accurately defined parameter because of the nature of the system: the region with lowest protein density is found at the solid interface, and that is where the oscillation begins.

Concentration Dependence. The oscillating nature of the protein density profile at the SAM/solution interface suggests a layering of the protein molecules induced by the presence of the hard boundary (substrate). This is characteristic of hard sphere layering near a hard wall.[37,38] Because it is expected that within the hard sphere model the packing density of the proteins (or hard spheres) has an impact on the oscillation period, further

(35) Gerstenberg, M.; Pedersen, J. *Langmuir* **2001**, *17*, 7040–7046.
(36) Gerstenberg, M.; Pedersen, J.; Majewski, J.; Smith, G. *Langmuir* **2002**, *18*, 4933–4943.
(37) Patra, C. N. *J. Chem. Phys.* **1999**, *111*, 6573–6578.
(38) Roth, R.; Dietrich, S. *Phys. Rev. E* **2000**, *62*, 6926–6936.
(39) Zhang, F.; Skoda, M.; Jacobs, R.; Zorn, S.; Martin, R.; Martin, C.; Clark, G.; Goerigk, G.; Schreiber, F. *J. Phys. Chem. A* **2007**, *111*, 12229–12237.
(40) Sun, C.; Yang, J.; Wu, X.; Huang, X.; Wang, F.; Liu, S. *Biophys. J.* **2005**, *88*, 3518–3524.
(41) Ferrer, M. L.; Duchowicz, R.; Carrasco, B.; de la Torre, J. G.; Acuna, A. U. *Biophys. J.* **2001**, *80*, 2422–2430.
(42) Schwendel, D.; Hayashi, T.; Dahint, R.; Pertsin, A.; Grunze, M.; Steitz, R.; Schreiber, F. *Langmuir* **2003**, *19*, 2284–2293.

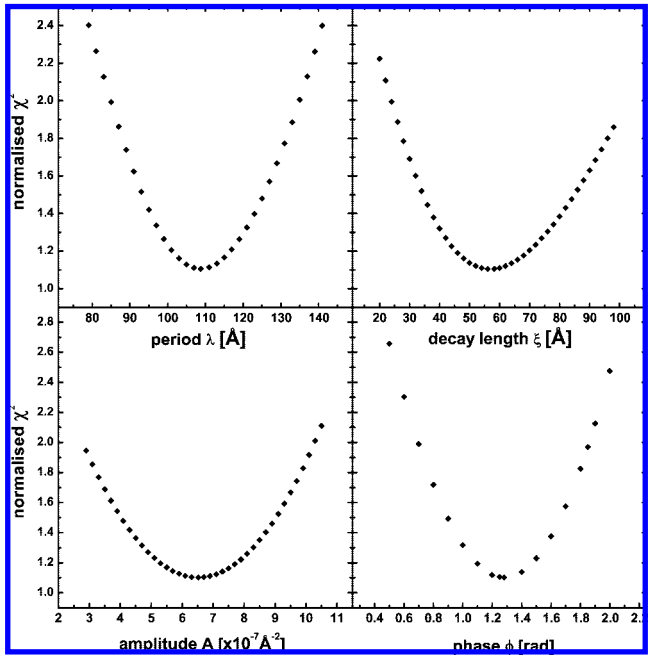

Figure 7. χ^2 distribution as a function of the following parameters: amplitude A, decay length ξ, and period and phase of the oscillation λ_p and ϕ, respectively.

Table 2. Parameters of the Fitted Oscillating Decays for an EG3OMe SAM in Contact with Protein Solutions of 15 and 27 wt % BSA Concentration[a]

BSA concentration	15 wt %	27 wt %
amplitude A ($\times$ 10^{-6} Å^{-2})	0.62	0.2
period λ_p (nm)	10.88	6.48
phase ϕ	2.3	2.2
decay length ξ (nm)	5.71	8.61
N_σ qualifier	6.91	1.64

[a] The low N_σ values in both cases indicate a good description by the fitted model.

measurements with higher protein concentrations were performed. Concentrations lower than 15 wt % turned out to be problematic because of insufficient contrast. Thus, a reflectivity measurement was performed with a higher BSA concentration (27 wt % BSA/D_2O/H_2O solution, data not shown). As before, the reflectivity profile could be fitted with an oscillating decay function at the SAM/solution interface. It is important to note that the period of the oscillation was reduced as a consequence of the higher protein density in solution: the average interparticle spacing is reduced. The decay length is increased at the same time (Table 2). This result further supports the hard sphere model assumption.

Salt Effects. Data from AFM experiments[19] suggest that the repulsive force exerted by the OEG SAM on the dissolved proteins has electrostatic contributions. This can be concluded from the fact that the measured forces scaled with the ionic strength of the solution according to the Derjaguin−Landau−Verwey−Overbeek (DLVO) theory.[43]

The ionic strength dependence was measured in a series of experiments using the same protein solution (15 wt % BSA in D_2O) and the same substrate. The following concentration steps were measured: 0 (the (intrinsic) ionic strength of a pure BSA solution is estimated to correspond to a 0.01 M NaCl solution as a consequence of dissolved amino acid residues), 0.05, 0.2, and 1.0 M. For each step, the protein solution was extracted from

(43) Israelachvili, J. *Intermolecular and Surface Forces*; Academic Press: New York, 1992.

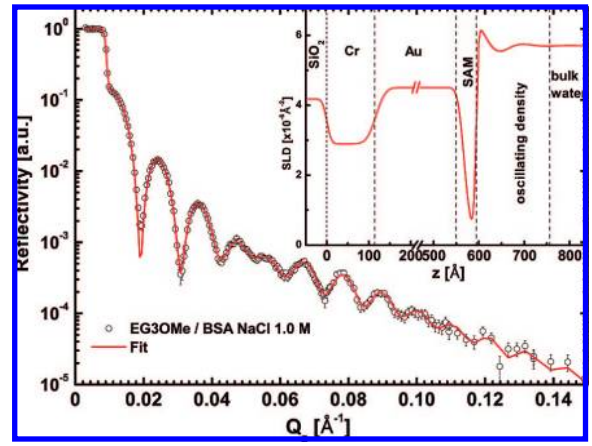

Figure 8. EG3OMe SAM in contact with a 15 wt % BSA solution at room temperature in a 1.0 M NaCl solution. For fit parameters, see Table 3.

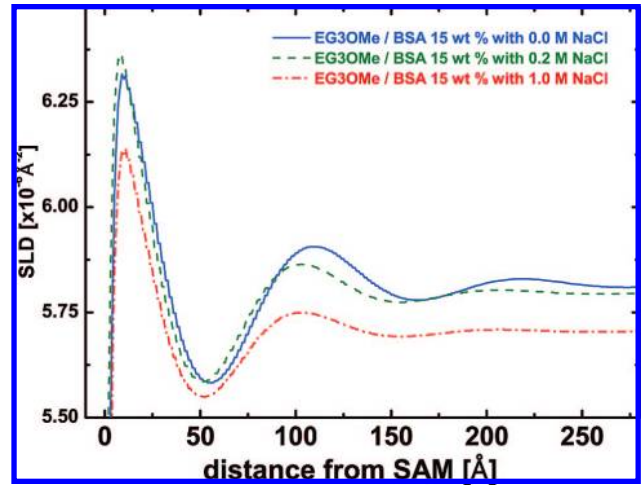

Figure 9. Oscillating protein density in the vicinity of an EG3OMe-terminated SAM for different NaCl concentrations in a 15 wt % BSA/D_2O solution. The lower bulk value for the 1.0 M solution is due to a slightly higher BSA concentration.

the sample cell, the volume was measured, and the appropriate amount of NaCl was added. Then, after the salt had dissolved, the solution was slowly reinjected into the sample cell. The sample was remounted and realigned, and the new measurement was started. As before, fitting of the reflectivity data revealed the typical oscillating protein density close to the SAM. Because measurements with no added salt have been shown in preceding sections, only the data, fit, and corresponding real-space profile for the measurement at 1.0 M salt concentration are shown in Figure 8. For the other salt concentrations, only the real-space profiles are shown in Figure 9.

The fitting parameters for a model with a sinusoidal decay are listed in Table 3 for three different salt concentrations. The amplitude, period, and decay constant are consistent with the previously described experiments on pure BSA solutions.

When the NaCl concentration is increased to 0.2 M, only small changes are visible in the reflectivity data. Accordingly, the subsequent fitting yields parameters very similar to those for the pure BSA solution. However, a slight trend toward smaller periods and stronger damping can be observed: the amplitude remains almost constant ((0.62−0.68) $\times$ 10^{-6} Å^{-2}), the period of the oscillation is slightly decreased from 10.8 to 10.3 nm, and the decay constant of the damping decreases to 4.6 nm from the

Table 3. Fit Parameters for an EG3OMe SAM in Contact with a 15 wt % BSA Solution at Room Temperature at Three Different NaCl Concentrations

layer	d (nm)	SLD ($\times 10^{-6}$ Å^{-2})	σ (nm)
quartz	n/a	4.18	n/a
Cr	11.71	2.89	0.86
Au	45.0	4.5	1.76
SAM	2.71	0.4	1.21
layer 0	0.2	5.82	0.4
0 M NaCl oscill. decay: $A = 0.62 \times 10^{-6}$ Å^{-2}, $\lambda_p = 10.88$ nm, $\phi = 2.3$, $\xi = 5.71$ nm			
0.2 M NaCl oscill. decay: $A = 0.68 \times 10^{-6}$ Å^{-2}, $\lambda_p = 10.34$ nm, $\phi = 1.28$, $\xi = 4.57$ nm			
1.0 M NaCl oscill. decay: $A = 0.56 \times 10^{-6}$ Å^{-2}, $\lambda_p = 10.29$ nm, $\phi = 1.32$, $\xi = 4.09$ nm			
bulk	n/a	5.77	0
0 M NaCl Hamilton: $b = 3$, $\nu = 216$; $R_{3,216,0.005} = 1.033$, $R = (\chi_1^2/\chi_{oscill}^2)^{1/2} = 1.345$			
0.2 M NaCl Hamilton: $b = 3$, $\nu = 224$; $R_{3,224,0.005} = 1.032$, $R = (\chi_1^2/\chi_{oscill}^2)^{1/2} = 1.220$			
1.0 M NaCl Hamilton: $b = 3$, $\nu = 216$; $R_{3,216,0.005} = 1.032$, $R = (\chi_1^2/\chi_{oscill}^2)^{1/2} = 1.157$			
0 M NaCl N_σ test: $N_\sigma^{oscill} = 2.04$, $N_\sigma^1 = 11.52$			
0.2 M NaCl N_σ test: $N_\sigma^{oscill} = 8.81$, $N_\sigma^1 = 17.5$			
1.0 M NaCl N_σ test: $N_\sigma^{oscill} = 4.49$, $N_\sigma^1 = 9.0$			

previous 5.7 nm. Upon increasing the NaCl concentration to 1.0 M, where the electrostatic interactions between the proteins (and between the proteins and the surface) are fully screened, the fitting values follow the same trend: the oscillation amplitude is now slightly lower at 0.56×10^{-6} Å^{-2}, the period is almost the same as for the 0.2 M solution, and the oscillation is more strongly damped, with $\xi \approx 4.1$ nm (Figure 8).

An overview of the protein density distribution in the vicinity of an EG3OMe-terminated self-assembled monolayer is presented in Figure 9. A clear trend toward less pronounced oscillations and a reduced period of oscillation at higher salt concentrations is visible, which is consistent with screened electrostatic interactions. However, the overall changes are small, with the largest deviations occurring at distances larger than 80 Å from the SAM, indicating that the observed effects are mostly due to screening effects in the bulk.[32] The additional fact that the protein-depleted region adjacent to the SAM, composed of reduced-density water, does not change significantly with increasing NaCl concentration suggests that the electrostatic contribution to the protein-repelling forces of the SAM is rather limited. These findings are in agreement with our small-angle scattering experiments on mixtures of OEG-SAM-protected Au colloids and proteins described in ref 39. It may be speculated that one major contribution to the nonfouling properties of OEG SAMs is the formation of a tightly bound hydration layer that is promoted by the structure and internal hydrophilicity of the SAM. An investigation into the properties of this potential hydration layer, however, is beyond the scope of this article.

Effect of Temperature. The results of Schwendel et al.[44] demonstrated that monolayers with slightly different chain lengths, in this case, EG3OMe- and EG6OMe-terminated ones, can show very different behavior when the temperature is changed. It was found that the protein resistance of EG3OMe monolayers is lost at temperatures lower than 11 °C and small amounts of adsorbed protein could be observed, whereas the EG6OMe SAM remained resistant even at lower temperatures. It should be noted that in the experiments of Schwendel et al.[44] fibrinogen was selected as a model protein to demonstrate protein adsorption at low temperature. In contrast, the neutron reflectivity measurements

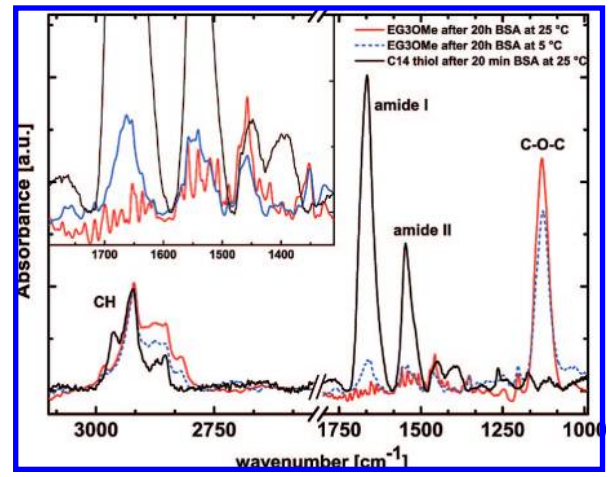

Figure 10. PMIRRAS data in air of two identical EG3OMe samples taken after 20 h of exposure to a 15 wt % BSA solution at room temperature (red solid line) and at 5 °C (blue dotted line). As a comparison, data is shown for a nonresistant C14 alkanethiol SAM after 20 min of exposure to a BSA solution (black line). The spectrum was normalized to the strongest CH stretching band. The adsorbed amount of BSA on the C14 alkanethiol SAM is much larger than on the low-temperature EG3OMe SAM. No adsorption was found on EG3OMe at room temperature.

presented here required the use of a protein with high solubility in water, such as BSA, in order to achieve the high concentrations necessary for a satisfactory SLD contrast. Therefore, the experiments of Schwendel et al. have been repeated using BSA. Figure 10 shows a comparison of EG3OMe SAMs exposed to a 15 wt % BSA/H_2O solution for 20 h at room temperature and at 5 °C. After the incubation time, the two identical samples were removed from their BSA solutions by slowly diluting the solution using copious amounts of ultrapure water of the same temperature. Finally, the samples were rinsed and blow dried in a soft argon stream. This procedure was necessary to prevent the accidental adsorption of BSA by Langmuir−Blodgett-like transfer when the samples were removed from the highly concentrated solutions. However, it also ensured that any remaining traces of BSA were irreversibly bound and could not be removed by rinsing. The dried samples were immediately measured using polarization modulation infrared reflectance absorbance spectroscopy (PMIRRAS).

BSA adsorption, characterized by the amide bands at 1550 and 1660 cm^{-1}, is clearly visible on the sample that was incubated at low temperature. The room-temperature sample shows only residual water vapor vibrations in the amide region. However, a comparison with a non-protein-resistant C14 alkanethiol sample that was exposed to the same BSA solution for 20 min at room temperature demonstrates that the adsorbed amount of BSA on the low-temperature EG3OMe sample is much smaller. To allow for a comparison of the adsorbed amounts on the low-temperature EG3OMe sample and on the reference alkanethiol sample, the spectra were normalized to the strongest CH stretching peak.

The corresponding neutron reflectivity experiments were performed in a temperature-adjustable cell using a water-cooled copper block in thermal contact with the sample cell. The temperature was regulated externally with a standard water chiller, and the cell temperature was monitored using an RDT (Pt100) sensor mounted inside the aluminum housing of the sample cell. The sample cell was mounted, and the temperature was set to 25 °C. After the system had equilibrated, the sample was aligned to the neutron beam, and the reflectivity was recorded (Figure 11). For the subsequent measurement at 5 °C, the temperature

(44) Schwendel, D.; Dahint, R.; Herrwerth, S.; Schloerholz, M.; Eck, W.; Grunze, M. *Langmuir* **2001**, *17*, 5717–5720.

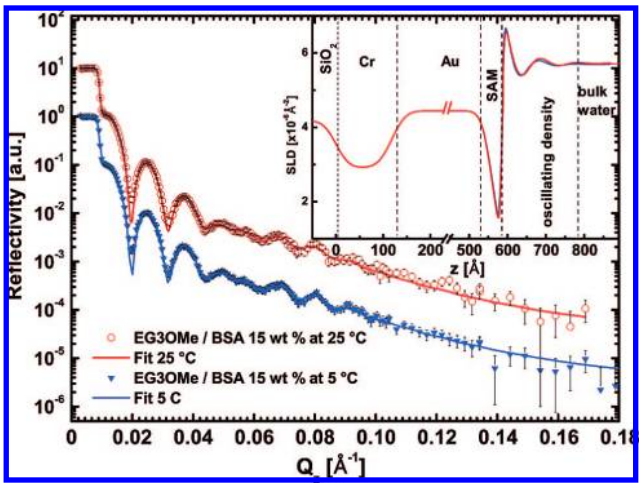

Figure 11. EG3OMe SAM in contact with a 15 wt % BSA solution at 25 °C (red open circles) and 5 °C (blue triangles). The curves are offset by a factor of 10 for clarity.

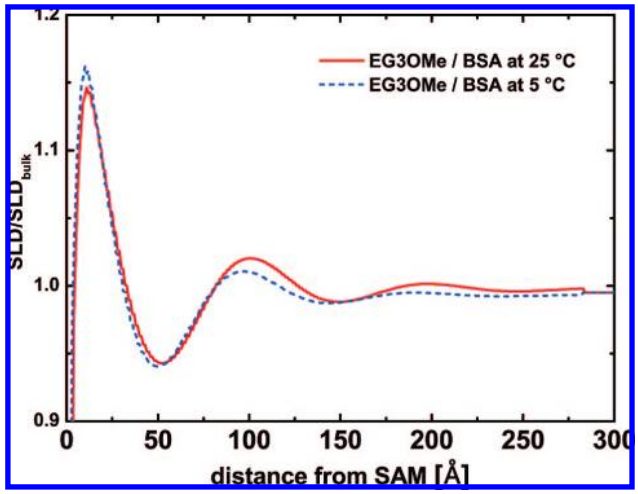

Figure 12. Comparison of the fitted protein density profiles at 25 °C (red line) and 5 °C (blue line) for an EG3OMe monolayer in contact with a 15 wt % BSA/D_2O solution.

was gradually lowered, and the sample was left to equilibrate for 1 h. The sample was then realigned to correct for potential thermal contraction of the cell. The temperature was monitored at regular intervals during the measurement and was kept constant with a maximum deviation of ±0.5 °C. Figure 11 shows the data, fit, and real-space profile for the EG3OMe sample in contact with a 15 wt % BSA/D_2O solution at 5 °C.

It was found that the oscillating structure of the protein density in the vicinity of the SAM persists down to a temperature of 5 °C, even though the amplitude, period, and decay length of the oscillation are slightly decreased (Figure 12). The first minimum in the scattering length density is lower at 5 °C, indicating a slightly higher density of proteins close to the SAM.

Conclusions

The density profile of a protein solution near a protein-resistant OEG-SAM-coated Au surface has been studied in detail using neutron reflectivity. It was found that the protein density oscillates around the bulk value by about ±15% of this value with a period of ~10 nm and that the oscillations are damped out quickly over a length of about 20 to 30 nm, with a decay constant of approximately 5 nm. The lowest protein density is found to be very close to the SAM, where in a region of 3 to 4 nm the scattering length density of the solution reaches a value of 90 to 98% of that of pure water. Whether this value is due to a small volume fraction of protein that is not excluded from that region or due to a reduced-density water layer as found in the measurements without proteins cannot be determined by this method. However, this region is strongly depleted of proteins. Further away from the SAM, it is followed by a region of about 4 to 5 nm, where the protein density is 5−8% higher than the bulk value. After that, the density oscillations are rapidly damped out until the protein concentration reaches its bulk value. The oscillating behavior of the protein density in the vicinity of the wall is characteristic of hard sphere layering near a hard wall.[37,38] The fact that the proteins are charged impacts only the effective hard sphere radius.[45]

The effects of temperature and ionic strength on the solution were also studied for this system. An increase in the NaCl concentration to 0.2 M leads to a slight decrease in the amplitude and period of the protein density oscillation. At a concentration of 1.0 M NaCl, the oscillation is almost completely damped out after 15 nm. However, the SLD and width of the protein-depleted layer adjacent to the SAM and the neighboring region with increased protein density hardly change even at a 1.0 M NaCl concentration. This shows that the interaction of proteins with the SAM is almost unaffected by the salt whereas the structure further away, in the bulk, is disturbed by the screening effect of the salt on the protein charge. This may indicate that the proteins reach the very proximity of the SAM but are prevented from adsorbing irreversibly, for instance, by a strongly bound hydration layer. Thus, it is suggested that electrostatic interactions do not appear to have a net effect on the phenomenon of protein resistance of OEG-terminated SAMs, although charges may play a more subtle role in the complex balance of forces within this intricate system.

The variation of temperature of the protein solution from room temperature to 5 °C caused little change in the measured density profile. A small reduction in the amplitude and period of the oscillation could be observed. No indication of protein adsorption could be found in situ. Thus, the breakdown of the protein resistance of EG3OMe-terminated SAMs at low temperature observed ex situ with PMIRRAS could not be confirmed by these in situ measurements. However, because the amount of adsorbed BSA found in the ex situ FTIR experiments was very small, it is conceivable that it was well below the sensitivity of the neutron reflectivity measurements. Alternatively, it may be speculated that the adsorption found ex situ is due to (marginal) Langmuir−Blodgett-like transfer during the rinsing and drying procedure or that adsorption of protein to areas containing defects in the SAM is promoted by the low-temperature environment.

It can be mentioned here that very recent advances in high-energy X-ray reflectivity[46] through liquids have demonstrated the feasibility of certain adsorption studies in situ, with sub-nanometer resolution. This may provide further insight into the very subtle mechanisms related to protein-resistant surfaces.

Acknowledgment. This work was supported by the Engineering and Physical Sciences Research Council (EPSRC), the Bundesministerium für Bildung und Forschung through the funding initiative Grossgeräteforschung (grant no. 03GRE1HD), and the Fonds der Chemischen Industrie.

LA8028534

(45) Bechinger, C. *Private communication*, 2007.
(46) Evers, F.; Shokuie, K.; Paulus, M.; Sternemann, C.; Czeslik, C.; Tolan, M. *Langmuir* **2008**, *24*, 10216–10221.